Nonlinear interplay of TEM and ITG turbulence and its effect on transport

2010 Nucl. Fusion 50 054005

(http://iopscience.iop.org/0029-5515/50/5/054005)

IOP Publishing and International Atomic Energy Agency Nuclear Fusion
Nucl. Fusion **50** (2010) 054005 (11pp) doi:10.1088/0029-5515/50/5/054005

Nonlinear interplay of TEM and ITG turbulence and its effect on transport

F. Merz and F. Jenko

Max-Planck-Institut für Plasmaphysik, EURATOM Association, Boltzmannstr. 2, 85748 Garching, Germany

E-mail: Florian.Merz@ipp.mpg.de

Received 17 July 2009, accepted for publication 15 March 2010
Published 21 April 2010
Online at stacks.iop.org/NF/50/054005

Abstract
The dominant source of anomalous transport in fusion plasmas on ion scales is turbulence driven by trapped electron modes (TEMs) and ion temperature gradient (ITG) modes. While the individual properties of each of these two instabilities and the corresponding microturbulence have been examined in detail in the past, the effects of a coexistence of the two modes and the phenomena of transitions between the TEM and ITG dominated regimes are not well studied. In many experimental situations, the temperature and density gradients support both microinstabilities simultaneously, so that transitional regimes are important for a detailed understanding of fusion plasmas. In this paper, this issue is addressed, using the gyrokinetic code GENE for a detailed investigation of the dominant and subdominant linear instabilities and the corresponding nonlinear system. A simple quasilinear model based on eigenvalue computations is presented which is shown to reproduce important features of the nonlinear TEM–ITG transition.

PACS numbers: 52.65.Tt, 52.30.Gz, 52.35.Ra

(Some figures in this article are in colour only in the electronic version)

1. Introduction

Most investigations of plasma microturbulence available in the literature focus on studying turbulence in an idealized limit, i.e. pure ion or electron temperature gradient (ITG/ETG) mode driven turbulence or trapped electron mode (TEM) turbulence. For the gyrokinetic simulations of the former two cases (see, e.g. [1, 2]), often the adiabatic electron/ion approximation has been used, which reduces the numerical effort considerably, but eliminates several physical aspects. One very important effect that occurs only with a gyrokinetic treatment of both species is TEM turbulence, which has been discussed, e.g., in [3–7] with $R/L_{T_i} = 0$, i.e. in an equally idealized limit as the ITG and ETG investigations cited above. For collisional TEM turbulence, the nonlinear interplay of unstable and stable modes has been addressed analytically in [8].

While it was important to isolate and study the various effects occurring in these regimes separately in a first step, eventually more realistic scenarios have to be considered, with gyrokinetic effects and gradients taken into account for both electrons and ions. ITG turbulence is often found to be the main cause of anomalous transport in fusion experiments. If the plasma conditions are chosen appropriately, it is also possible to experimentally investigate 'pure' TEM regimes and compare with turbulence simulations [3, 9]. But in more conventional situations, the application of several heating methods (ECRH plus neutral beam injection (NBI)) and/or a sufficiently high collisionality leads to finite (and often similar) values for the temperature gradients of all species, which usually means that several linear instabilities are present simultaneously.

There has been some recent work on the interplay between ETG and ITG turbulence, which exist on different spatio-temporal scales [10–12]. However, even in parameter ranges where ETG modes are stable, there is the possibility of a coexistence of different modes, namely TEM and ITG instabilities, which have comparable spatial scales, comparable linear growth rates but in general different real frequencies. There have been linear studies of the TEM–ITG transition using an eigenvalue solver [13] and nonlinear simulations of combined TEM–ITG turbulence [14, 15], with the latter reference comparing global gyrokinetic simulations with experiments. A number of quasilinear investigations of TEM–ITG turbulence based on initial value computations is also available [16–18].

With the gyrokinetic code GENE [2, 4] it is possible to perform linear eigenvalue computations [19], which allow for detailed investigations of dominant and subdominant microinstabilities, as well as nonlinear turbulence simulations. This feature is used in this paper for a thorough study of the linear and nonlinear coexistence of TEM and ITG modes in

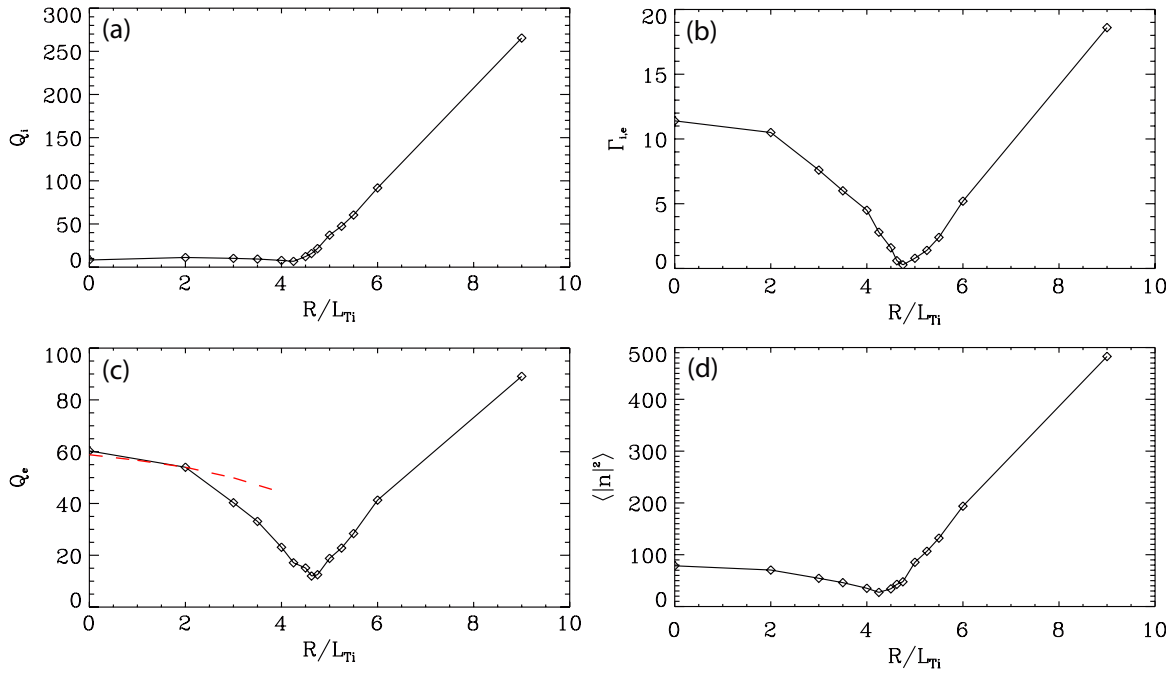

Figure 1. Ion and electron heat (a), (c) and particle (b) fluxes and the fluctuation level (d) as a function of the ITG. The dashed curve in (c) corresponds to the TEM transport model described in [6].

the transition region between the 'pure' collisionless TEM and ITG regimes.

The interaction between the different unstable modes at the TEM–ITG transition produces some interesting phenomena, including a suppression mechanism for the particle flux. This is of importance because the particle flux in gyrokinetic simulations using experimentally measured profiles is often too high, which could be caused by a detuning of the suppression mechanism due to the substantial uncertainties in the gradients obtained from these measured profiles. Some of these features can be understood at least qualitatively by quasilinear investigations, which offer the possibility for extended parameter scans.

The rest of this paper is organized as follows: in the next section, we describe the setup for the linear and nonlinear simulations. In section 3, results of a nonlinear scan from pure TEM turbulence to ITG dominated turbulence are presented and compared with linear eigenvalue simulations; some interesting properties of the turbulence exactly at the transition are studied in detail. Section 4 introduces a simple quasilinear model of the TEM–ITG transition based on eigenvalue computations. This model is then used for higher dimensional parameter scans and tested with another nonlinear parameter scan in section 5. All findings are summarized in the last section of this paper.

2. Setup for the simulations

All the simulations presented in this paper have been performed with the GENE code [2, 4] in $\hat{s}$–α geometry with $q_0 = 1.4$, $\hat{s} = 0.8$ and $\epsilon \equiv r/R = 0.16$. A small but finite $\beta = 10^{-3}$ is used, which suppresses the high-frequency electrostatic shear-Alfvén waves (and therefore reduces the numerical effort), but does not lead to electromagnetic effects on the growth rates or transport, so that the simulations can be considered electrostatic. Consequently, the Shafranov shift is set to $\alpha = 0$. The temperature ratio of the two plasma species is set to $T_e/T_i = 2$; furthermore, a reduced mass ratio of $m_e/m_i = 1/400$ is used. Due to the temperature ratio, which can be achieved experimentally with dominant electron heating, the ETG modes are suppressed in a wide region of the $(R/L_{T_e}, R/L_{T_i}, R/L_n)$ parameter space, so that the perpendicular resolution of the nonlinear simulations can be limited to ion scales. Collisions are neglected for simplicity, the remaining instabilities are thus collisionless TEMs (CTEMs) and ITG modes. In the parameter range considered here, the two instabilities can always be identified unambiguously by the sign of their real frequency. The perpendicular box size for the nonlinear simulations is $L_x = 150\rho_s$ and $L_y = 125\rho_s$, the numerical resolution is $128 \times 64 \times 24 \times 48 \times 8$ points in the radial, binormal, parallel, $v_\parallel$, and μ directions, respectively, and both electrons and ions are retained. For the linear computations the perpendicular box sizes are adapted in order to obtain the maximum number of poloidal connections, the number of radial modes is reduced to five and all other parameters are kept fixed at the values of the nonlinear simulations. All growth rates and frequencies are normalized to c_s/R with $c_s = \sqrt{T_e/m_i}$, the binormal wavenumber k_y is normalized to $\rho_s = \sqrt{T_e m_i}/eB_0$, the particle fluxes to $n_e c_s(\rho_s/R)^2$ and the heat fluxes to $p_e c_s(\rho_s/R)^2$.

3. Nonlinear results and comparison with linear behaviour

To study the transition between the TEM and ITG turbulence regimes, a scan of the normalized ion temperature gradient R/L_{Ti} at fixed normalized electron temperature and density gradients $R/L_{T_e} = 4.5$, $R/L_n = 3$ is performed. Figure 1 shows the nonlinear particle (b) and heat fluxes for ions (a)

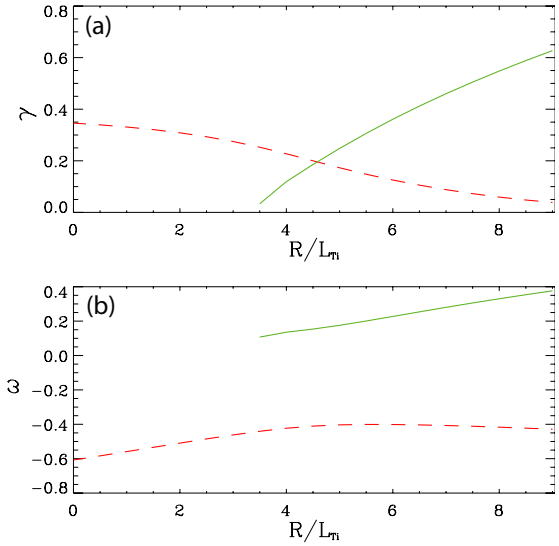

Figure 2. The linear growth rates γ (a) and frequencies ω (b) of the TEM (dashed) and ITG mode for a 'characteristic' wavelength of $k_y = 0.25$. The modes are clearly distinguishable by the sign of their frequency over the full parameter range.

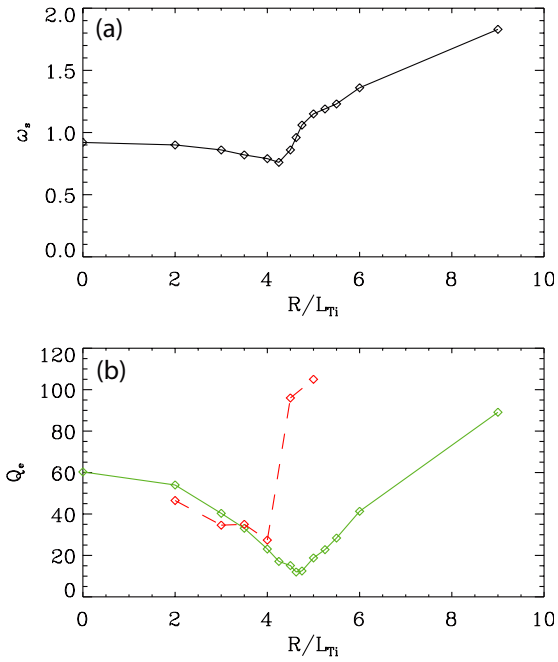

Figure 3. Shearing rate ω_s (a) and electron heat flux Q_e (b) as a function of R/L_{T_i}. Continuous lines correspond to full nonlinear simulations, for the dashed curve, the zonal flows have been artificially suppressed.

and electrons (c) as well as the average squared fluctuation density (d) as a measure of the fluctuation level.

The plots show a clear outward particle transport at both end points of the scan, a large TEM induced electron heat transport for low R/L_{T_i} and a very strong ion heat transport for the ITG dominated end of the scan. The most interesting feature which is common to all four plots is a minimum at $R/L_{T_i} \approx 4.6$. This is approximately the transition point between TEM and ITG turbulence, which can be seen in figure 2, where the R/L_{T_i} dependence of the two linear instabilities at a typical k_y of 0.25 is depicted. This linear scan shows a critical gradient for the ITG instability of $R/L_{T_i} \approx 3.3$ and a relatively slow decay of the TEM growth rate with the ITG, with TEM subdominantly unstable even for the highest R/L_{T_i}. The modes can be clearly distinguished by their diamagnetic drift direction (i.e. the sign of their frequency, see also figure 4(b)) for all parameters used in this paper. The minimum in the nonlinear R/L_{T_i} scan is also visible in the fluctuation amplitude, which can be partly explained by the minimum of the growth rate at the transition point. This of course contributes to the minimum in the fluxes, but has to be accompanied by a corresponding change in the relative phases angles which enter the fluxes to account for the observed magnitude of the effect.

The fact that the TEM/ITG transition occurs very close to the minimum of the fluxes at $R/L_{T_i} \approx 4.625$ is also confirmed by a rather abrupt change in the relevance of zonal flows. Figure 3(a) shows the shearing rate

$$\omega_s = \langle\langle|\partial_x^2 \phi_{\text{zonal}}|^2\rangle_x^{1/2}\rangle_t$$

(brackets denote averaging with respect to their subscript) as a function of R/L_{T_i}, displaying a sudden increase at $R/L_{T_i} \approx 4.25$, i.e. slightly below the TEM/ITG transition, but well above the linear critical gradient for ITG modes. Figure 3(b) shows this more clearly: as described in [4–7], zonal flows do not play a decisive role in the saturation of pure temperature gradient driven TEM turbulence with $T_e > T_i$ and $\eta_e = L_n/L_{T_e} > 1$ as considered in this paper. The transport levels of the saturated phase stay almost constant even when the zonal flows are artificially suppressed, as is shown in the dashed curve of figure 3(b). For low values of R/L_{T_i}, the curves with and without zonal flows are virtually identical, but this changes drastically when the ITG modes start to become the dominant drive of the system—then the zonal flow suppression leads to an increase in the electron heat transport of a factor five or more, as reported in the literature for the pure ITG regime [20–22].

The transition in the zonal flow dependence coincides with the rise in the ion heat flux. Interestingly, these changes occur at a value that is significantly higher than the linear critical R/L_{T_i} for the onset of ITG instability. As can be observed by comparing the linear results in figure 2 with the behaviour of the nonlinear fluxes and the zonal flows (figures 1 and 3), the nonlinear critical gradient is shifted from its linear value of $R/L_{T_i} \approx 3.3$ to $R/L_{T_i} \approx 4.0$. This implies that the saturation mechanism that stabilizes the TEM turbulence also works for weakly unstable ITG modes. However, the decrease in the TEM activity with R/L_{T_i} due to smaller growth rates, combined with a simultaneous increase in ITG growth rates, obviously leads to a situation where this TEM induced stabilization is no longer possible and the ITG generated zonal flows take over that role.

While these global features of the fluxes demonstrate the presence of nontrivial effects at the transition point between TEM and ITG turbulence, for a deeper understanding, the spectral dependence has to be taken into account. In figure 4, the linear growth rates and frequencies are shown as functions of the two-dimensional parameter space (k_y, R/L_{T_i}). The plot shows that for a wide range of parameters, both instabilities are present simultaneously. Furthermore, the intersection of

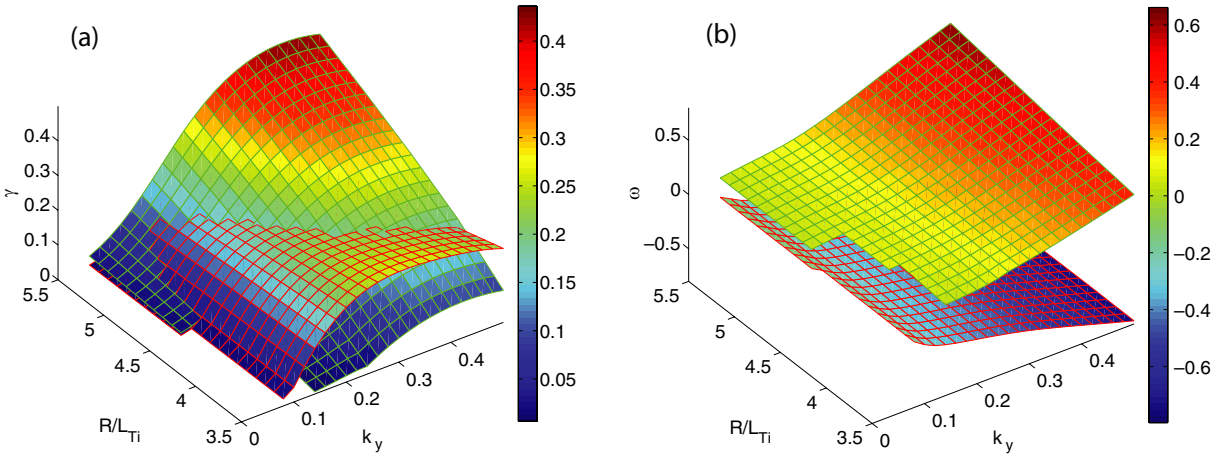

Figure 4. Linear growth rates (a) and frequencies (b) as a function of K_y and R/L_{Ti}. The TEM and ITG modes are distinguishable by the dark and light (red and green) colour of the mesh, respectively. The missing patch at low k_y and R/L_{T_i} is due to the stability of the ITG mode for these parameter values.

the two surfaces describing the growth rates of the different modes is not parallel to the k_y axis (also see figure 7(b)). It rather describes a curved line, with the R/L_{T_i} of the transition first increasing up to $k_y = 0.15$ and then decreasing with k_y, implying that for some rather large range in R/L_{T_i}, the dominant microinstability is different for different k_y. This means that at least linearly, the TEM/ITG transition takes place gradually and for a quite extended parameter range, a coexistence between TEM and ITG modes is to be expected.

It is *a priori* not clear that a higher growth rate leads to a higher amplitude (i.e. dominance) of the mode in the saturated turbulent regime, i.e. whether the linear findings are decisive for the nonlinear simulations on that issue. If the nonlinear damping mechanism is different for the two instabilities (as is strongly suggested by figure 3), it is well possible that a linearly subdominant mode, although growing slower in the initial phase of the simulation, ends up at a higher saturation level and thus dominates the system.

To determine the role of the different modes for the different perpendicular wavenumbers, it is useful to analyse the frequencies of the turbulent fluctuations. A windowed Fourier transform is applied to the time traces of all perpendicular modes of the perturbed density field and the result is averaged over the radial and parallel directions to obtain the averaged nonlinear spectral density $D(\omega, k_y)$.

Figure 5(a) shows the k_y dependence of the spectral density for the $R/L_{T_i} = 4.625$ case. For this plot, $D(\omega, k_y)$ has been normalized to $\sum_\omega D(\omega, k_y)$ for each k_y in order to remove the strong variation with k_y which would otherwise obscure the variation with ω. The normalized spectral density is colour coded, the dashed (red) and continuous (green) lines indicate the frequencies of the linear TEM and ITG modes for comparison. Figure 5(b) shows the corresponding growth rates of the two microinstabilities. The nonlinear result reveals that while the TEM contribution dominates for $0.1 < k_y \leqslant 0.2$ and the ITG contribution is dominant for $k_y \geqslant 0.25$ and $k_y = 0.05$, TEM and ITG turbulence can coexist not only at different k_y in the same simulation but even at the same perpendicular wavenumber, with the remnants of the two microinstabilities interpenetrating and drifting in opposite directions, at a frequency that is practically unaltered with respect to the linear computations. The linear k_y values where the growth rates of the two instabilities intersect and the nonlinear values where the dominant frequency changes sign are not distinguishable ($k_y \approx 0.1$ and $k_y \approx 0.22$ in both cases), implying that the properties of the turbulence are largely set by the linear physics also on this issue. This phenomenon might be accessible experimentally by means of Doppler reflectometry (see, e.g., [23]).

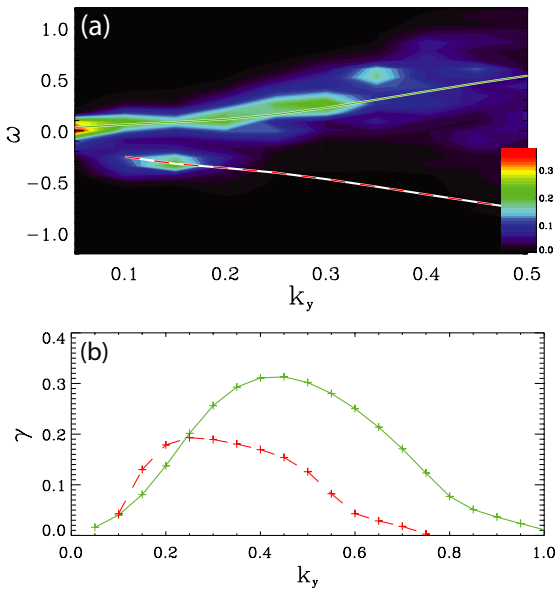

Figure 5. (a) Normalized nonlinear frequency spectrum (colour coded) as function of k_y for $R/L_{T_i} = 4.625$; the dashed (red) and continuous (green) lines are the linear frequencies for TEM and ITG modes respectively. (b) The corresponding linear growth rates.

Note that the distribution function of the frequencies becomes broader with increasing k_y and the peaks at the linear eigenfrequencies become less pronounced, indicating that the linear drive plays a less decisive role for $k_y \gtrsim 0.5$, but since TEM and ITG mode driven turbulence does not produce much transport on these scales, we focus on the low k_y range.

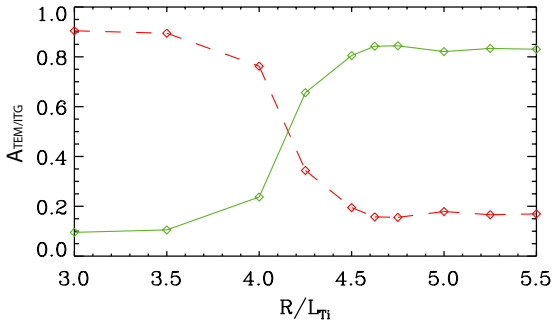

Figure 6. Normalized TEM (dashed line) and ITG (continuous line) contributions as defined in equation (1) as a function of R/L_{T_i}.

As is shown in figure 5(a), the amplitude spectrum of the Fourier decomposition shows two structures which are well separated by a minimum at $\omega \approx -0.1$. As a measure for the relative importance of the different instabilities for the nonlinear simulation, we use $k_y = 0.25$ as a 'representative' wavenumber and compute the normalized sum over the negative frequency peak of the spectral density,

$$A_{\mathrm{TEM}} = \frac{\sum_{\omega \leqslant -0.1} D(\omega, k_y = 0.25)}{\sum_{\omega} D(\omega, k_y = 0.25)} \qquad (1)$$

and attribute it to the TEM mode. The amplitude of the ITG contribution A_{ITG} is defined equivalently as the normalized sum over the positive frequency peak ($\omega > -0.1$). This criterion is of course not strict, since the tails of the frequency distributions of TEM and ITG turbulence can leak into the other frequency range. The result as a function of R/L_{T_i} is shown in figure 6. The plot reveals a very clear transition between a regime with ≈90% TEM contribution for $R/L_{T_i} \leqslant 3.5$ and ≈85% ITG contribution for $R/L_{T_i} \geqslant 4.625$. However, there is a transition range where both instabilities act at the same perpendicular wavenumber; the two contributions are equal for $R/L_{T_i} \approx 4.2$.

Since the TEM–ITG transition is reasonably sharp, it is possible to get an indication of which microinstability dominates the turbulence from the averaged frequency $\bar{\omega} = (\sum_{\omega} \omega D(\omega, k_y))/(\sum_{\omega} D(\omega, k_y))$. Since the ITG and TEM peaks in the frequency distribution are not exactly symmetric with respect to the origin, a value of $\bar{\omega} = 0$ does not exactly correspond to equal amplitudes of TEM and ITG contributions, but this criterion can nevertheless be used as a reasonable identification mark for the transition. The result is shown in figure 7(a), where the average frequency is depicted as a function of $(k_y, R/L_{T_i})$. The transition is quite clearly visible in the colour coding, additionally the $\bar{\omega} = 0$ contour line has been marked in black. Due to the finiteness of the data set for the computation of the frequency distribution and the crudeness of the $\bar{\omega} = 0$ criterion, the plot and the line are subject to noise, but the comparison with figure 7(b) again displays a remarkable similarity of the linear and nonlinear behaviour, clearly showing that the coexistence of TEM and ITG mode turbulence at different k_y is very common if R/L_{Te} and R/L_{Ti} are in the same range.

After this discussion of the general features of the TEM–ITG transition, a detailed investigation of the most intriguing feature of figure 1, namely the clear minima in the transport quantities at the TEM–ITG transition, is in order. Of special interest in this context is the particle flux, as will be discussed in more detail in section 5. To reveal the mechanism that creates this minimum at $R/L_{T_i} = 4.625$, the spectral decomposition of the fluxes is shown in figure 8. Plot 8(a) shows that the TEM turbulence, which is predominant at $0.1 \leqslant k_y \leqslant 0.2$, leads to an outward particle transport, this contribution is balanced by the particle pinch of the ITG turbulence at $0.2 < k_y < 0.4$; the contributions from even higher (or lower) k_y can be neglected. The particle flux shows a zero-crossing very close to the k_y values where the growth rates of the two underlying microinstabilities intersect and the frequency distribution shows comparable TEM and ITG contributions, implying that the same balancing of inward and outward flux can not only work globally for the whole system, but even for one specific k_y contribution. Together this implies that the phenomenon of approximately zero global particle flux observed in this nonlinear simulation is the result of a fine tuning of the effects of the TEM and ITG contributions at different k_y. A spectral dependence of the sign of the anomalous particle transport has also been observed in [14].

The other plots of figure 8 show that the spectral separation of dominant ITG and TEM turbulence also causes a double peak in Q_{e} and can be confirmed by other characteristic properties such as the ratio of ion and electron heat flux, which has typical values for TEM turbulence at $k_y \approx 0.15$ and typical ITG values at $k_y \approx 0.3$.

4. Construction of a quasilinear model for the flux ratios

For temperature gradient driven TEM turbulence, a quasilinear transport model was described in [6, 24, 25]. This model, which was used to create the dashed line in figure 1(c), ignores subdominant contributions and has been applied to pure TEM cases in the past. As can be seen in the plot, it describes the nonlinear parameter dependences of the electron heat flux to a good degree for the pure TEM regime, but deviates from the nonlinear values when subdominant ITG contributions start to appear, which was to be expected.

Nevertheless, it has been shown in the last section that the turbulence inherits many features of the microinstabilities, even in the TEM–ITG transition region. It is therefore conceivable that a quasilinear description is sufficient for some qualitative investigations.

For the almost electrostatic cases considered here, the heat and particle fluxes are determined by the amplitudes of the corresponding moment of the distribution function and of the electrostatic potential and the phase angle between these two quantities. While the saturation amplitude and therefore the absolute value of the heat and particle fluxes can only be determined by nonlinear simulations, an unambiguous value for the sign and the ratio of the different fluxes, $Q_{\mathrm{i}}/Q_{\mathrm{e}}$, Γ/Q_{e}, Γ/Q_{i}, can be determined already from linear computations.

From the last section it is clear that estimating the amplitude ratio of the two coexisting modes at a given k_y is not completely straightforward, but it seems plausible to make the ansatz that the amplitude of the two modes at a given k_y is a monotonically increasing function of the respective growth

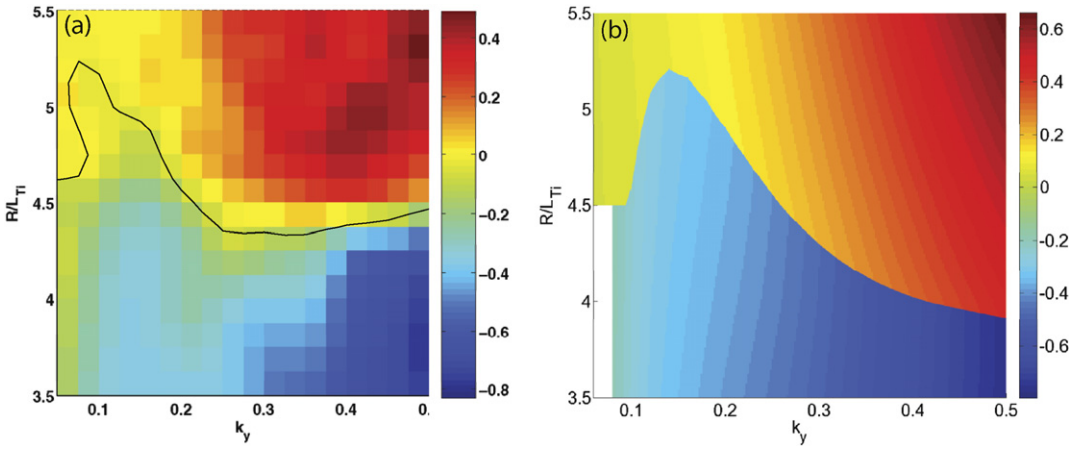

Figure 7. (*a*) Averaged nonlinear frequency $\bar{\omega}$ (colour coded), the $\bar{\omega} = 0$ contour line (black) may be used to mark the TEM–ITG transition. (*b*) The corresponding frequencies of the dominant linear microinstability.

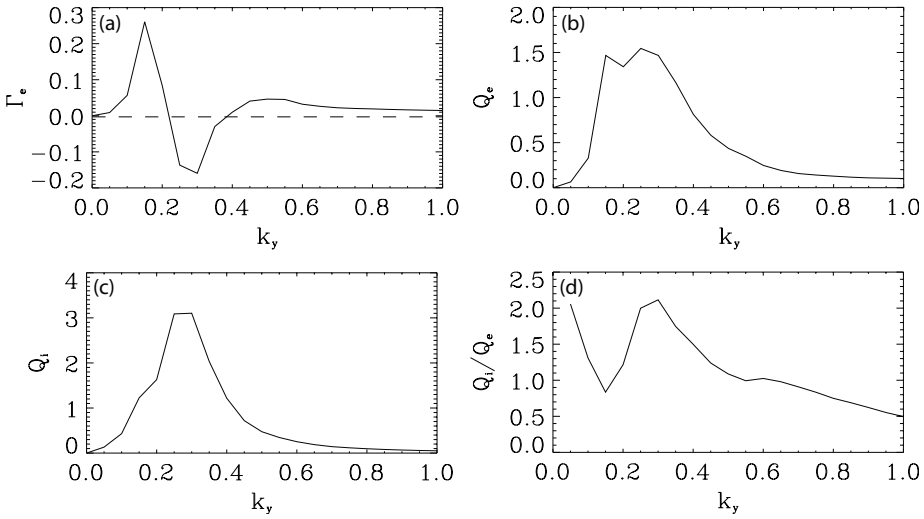

Figure 8. Particle flux (*a*), electron and ion heat fluxes (*b*), (*c*) and the ratio of the ion and electron heat fluxes (*d*) as a function of k_y for $R/L_{T_i} = 4.625$. The dashed line in (*a*) corresponds to $\Gamma = 0$.

rate. This is of course not exactly true, as can be concluded from the comparison of figures 2 and 6, but it may still serve as an approximation. Another problem is the weighting of the different k_y contributions in the system. As discussed in the last section, the ratio of the amplitudes/growth rates of the two instabilities is sensitive to the k_y value chosen. Since a nonlinear simulation contains many different k_y contributions with different amplitudes, it is difficult to find an appropriate prescription for the superposition of different linear modes in a quasilinear model.

In order to arrive at a simple quasilinear model that allows for extensive parameter scans, the problem of the weighting of the different k_y contributions is circumvented by using only one, 'characteristic' k_y, similar to the approach followed in [17]. This is of course a crude approximation, but as has been discussed in the last section, the same coexistence of modes that influences, e.g., the particle transport in the full system also occurs at a single k_y. If this value of k_y is chosen carefully, the TEM and ITG contributions at that k_y value approximately represent the summed contributions from lower and higher k_y, so that this 'central' mode reflects the whole system. A suitable choice for this mode is, as it turns out, $k_y = 0.25$. As mentioned above, a method to combine the contributions from the two microinstabilities has to be prescribed; an obvious starting point for the weighting factors to combine the flux ratios computed from TEM and ITG modes is the powers of the respective growth rates:

$$R_m = \frac{\gamma_{\mathrm{TEM}}^p R_{\mathrm{TEM}} + \gamma_{\mathrm{ITG}}^p R_{\mathrm{ITG}}}{\gamma_{\mathrm{TEM}}^p + \gamma_{\mathrm{ITG}}^p}, \tag{2}$$

with $R = (Q_\mathrm{i}/Q_\mathrm{e}, \Gamma/Q_\mathrm{e}, \Gamma/Q_\mathrm{i})$. A suitable value for the exponent p has been determined by comparison of the resulting quasilinear flux ratios with the nonlinear values, the result for $p = 10$ is shown in figure 9.

Given the crude approximations, the agreement between the respective curves is quite good. It is obvious that all basic features such as the position of the minima, turning points and even the approximate values of the curves are well described by the quasilinear approximation. The most significant deviation is that the value of the minimum of the particle flux is underestimated by the model, predicting a particle pinch instead of a small remaining outward transport.

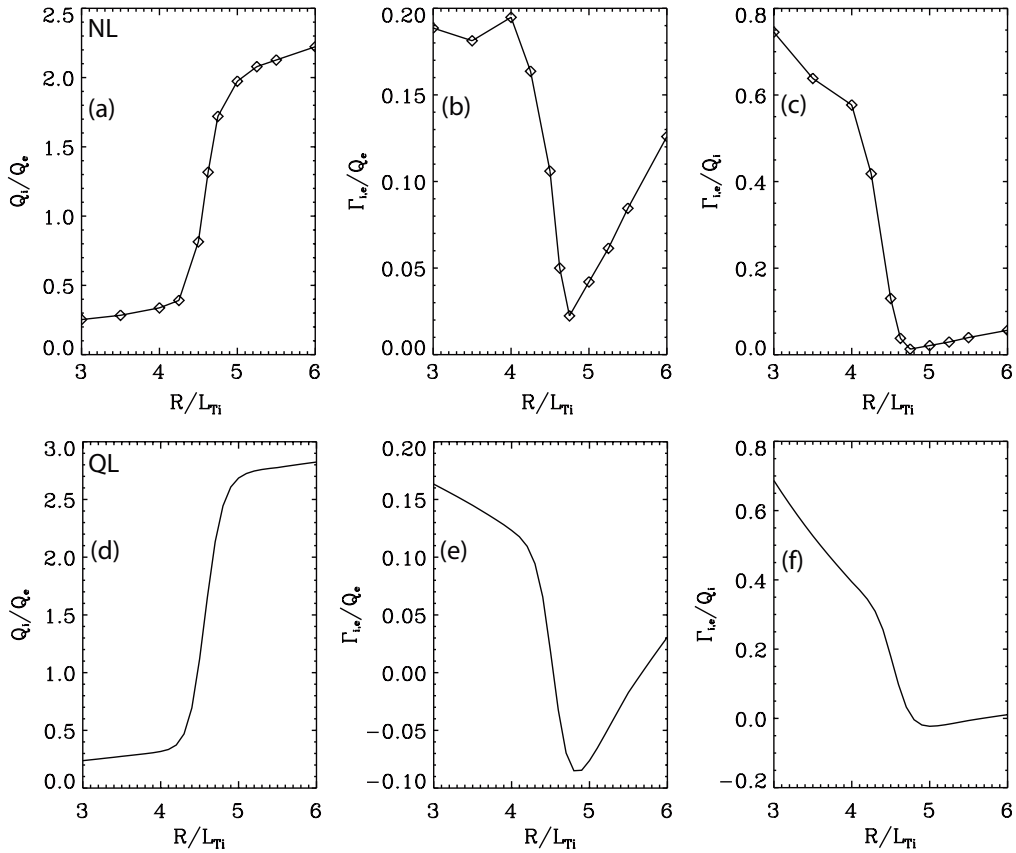

Figure 9. Nonlinear flux ratios (top) versus quasilinear flux ratios (bottom) as defined by equation (2).

Nevertheless, this quasilinear model seems to be able to describe the basic features correctly and will therefore be used to try to understand some parameter dependences by simple and fast linear computations. Note that there have been quasilinear gyrokinetic investigations of TEM/ITG turbulence before [16], but because an initial value solver was used for the computations, the subdominant modes have not been accessible, resulting in a discontinuity of the quasilinear predictions at the linear TEM–ITG transition—which is of course unphysical and difficult to interpret. Furthermore, initial value computations become increasingly difficult close to mode transitions, as the amplitudes of the two exponentially growing modes take longer and longer to separate. Since this separation of the amplitudes is the prerequisite for convergence of the initial value solver, the computation time diverges at the mode transition, indicating the superiority of eigenvalue computations for this kind of investigations. A quasilinear approach based on eigenvalue computations is also used successfully in recent gyrofluid models [26].

5. Application and test of the quasilinear model

The model defined in the last section does not predict the values of the transport fluxes, but only their ratios. This may seem not very useful at first glance, but has one very important application, namely the prediction of the zero-crossing of the particle flux.

To realize the relevance of this, it is important to understand that in the widely used local δf approximation, which underlies all nonlinear simulations presented in this paper, the average background gradients (R/L_n, R/L_{T_e}, R/L_{T_i}) driving the turbulence are held constant throughout a simulation. They are, in particular, independent of the transport fluxes (Γ, Q_e, Q_i), which constitute the main output of such simulations.

The fluxes in a real fusion experiment, on the other hand, are dictated by the output of the heating and refuelling systems; the values for the gradients, which adjust more or less freely to meet these constraints on the fluxes, are obtained experimentally from a combination of direct experimental measurements and a MHD reconstruction of the equilibrium. This procedure usually leads to quite substantial error bars (several 10%) in the gradients, while the values for the fluxes are much more accurate. There are of course also uncertainties for other parameters such as the β, $\hat{s}$ or the temperature ratio, but the simulated fluxes are, in general, much less sensitive to changes of these parameters than of the gradients.

The combination of these two points implies that it can be difficult to directly compare simulations and experiments, especially close to critical gradients, where small variations (or inaccuracies) of the gradients can lead to big variations of the computed fluxes. If the three fluxes in all points of the three-dimensional parameter space of the gradients could be computed, this information could be used to match the experimental fluxes and make a prediction for the gradients, allowing for much more robust comparisons with experimental data. Since this is out of scope for nonlinear simulations, it is important to find reliable quasilinear descriptions

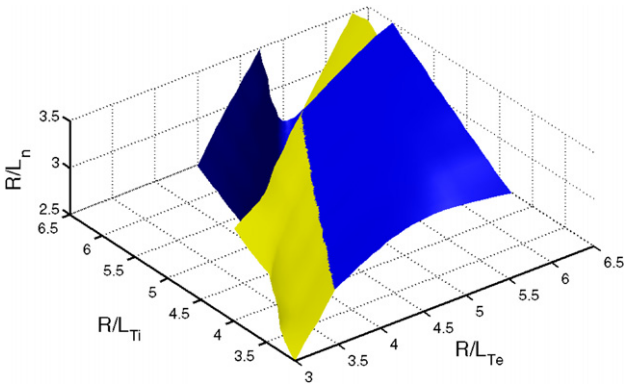

Figure 10. The $\Gamma \approx 0$ surface (dark/blue shading) as predicted by the quasilinear model defined in section 4, and the ITG–TEM transition surface (light/yellow shading) for the 'typical' $k_y = 0.25$ mode. The region with the particle pinch is 'behind' the blue surface in this view.

that at least partially allow for the comparisons described above.

An especially interesting (and accessible) subject for this kind of investigations is the particle flux. While all fusion experiments have strong heating systems which deposit their energy close to the magnetic axis and can therefore sustain significant radial heat fluxes, the possibilities of refuelling particles at the plasma centre are limited. The pellet injection systems used for that purpose are pulsed and are not able to change the quasi-stationary particle fluxes significantly, and also the NBI systems that are used for heating have no significant impact, so that $\Gamma \approx 0$ has to be fulfilled for all experimentally accessible situations [16]. If neoclassical effects such as the Ware pinch can be neglected, the particle flux can be identified with the turbulent particle flux, which has very advantageous implications for quasilinear models. While it is difficult to predict the absolute value of the transport, the prediction of the sign of the transport (or transport ratio), and thus its zero-crossing in parameter space, is much easier. This also holds for very simple quasilinear models such as the one presented in the last section.

If the fluxes vary smoothly with all parameters of the system (as is expected), the $\Gamma \approx 0$ condition defines a hypersurface with one dimension less than the parameter space under consideration (i.e. it has codimension one). If the parameter space is restricted to the most important parameters for the fluxes, namely the gradient triple $(R/L_n, R/L_{T_e}, R/L_{T_i})$, the $\Gamma \approx 0$ condition is fulfilled on a two-dimensional surface in parameter space. In previous quasilinear studies considering only dominant linear contributions [16], only low dimensional cuts of this hypersurface have been shown, but with the model based on eigenvalue computations defined in the last section and the possibility of extended parameter scans in GENE, it is now possible to compute the hypersurface in higher dimensions.

To demonstrate this, a three-dimensional linear scan of the gradients R/L_{T_e}, R/L_{T_i}, R/L_n was used to compute the quasilinear $\Gamma \approx 0$ surface (dark/blue shading) in figure 10. It shows that the parameter dependences are far from trivial; the blue surface, which separates the region exhibiting a particle pinch from the region with outward particle transport, is not aligned with any of the axes, so that for a minimization of the particle transport, the dependence on all three gradients has to be taken into account. The $\Gamma \approx 0$ surface consists of two 'wings'. The right one appears in the proximity of and more or less parallel to the light/yellow surface that represents the linear TEM–ITG transition of the $k_y = 0.25$ mode; it corresponds to the balance of TEM induced outward and ITG induced inward particle transport that was discussed in section 3. For the left wing, however, the TEM growth rate is too small to affect the system; the zero particle flux in this case arises due to a change of sign of the ITG contribution itself.

The nonlinear scan presented in section 3 corresponds to a line with $R/L_{T_e} = 4.5$ and $R/L_n = 3.0$ in this three-dimensional plot, slightly cutting through the blue surface very close to the TEM–ITG transition. If this line is shifted to a slightly higher R/L_{Te} or slightly lower R/L_n, the quasilinear model predicts a particle pinch in a range of R/L_{T_i} values.

To test this prediction and examine the nature of the second zero-crossing of the particle flux, another nonlinear scan with again $R/L_{T_e} = 4.5$ but $R/L_n = 2.5$ has been performed. The transport fluxes, which indeed confirm the existence of a particle pinch, are shown in figure 11. The curves largely resemble the $R/L_n = 3$ case of figure 1, except that the electron heat flux on the TEM dominated low R/L_{T_e} side is significantly lower due to a decrease of the TEM growth rates and the particle flux is generally reduced and shifted to negative values by almost two units.

For a detailed analysis of the predictions of the quasilinear model, figure 12 shows the nonlinear and quasilinear flux ratios for the $R/L_n = 2.5$ case (black curves). It is obvious that the model describes the basic features also in this case, e.g. the position (and its shift in R/L_{T_i} with respect to the $R/L_n = 3$ case) of the turning point of the Q_i/Q_e curve, which might be used as a definition of the TEM/ITG transition, or the positions of the transport minima.

The dotted and dashed curves in the quasilinear plots (d)–(f) show the values computed from the 'pure' TEM and ITG modes, respectively. The plots involving the particle flux confirm the above statement on the causes for vanishing particle flux. While the first zero-crossing is caused by the coexistence of TEM and ITG modes with opposite transport directions, the second is due to a change in the transport direction of the ITG contribution alone. To confirm this also nonlinearly, the transport spectra for the $R/L_n = 2.5$, $R/L_{T_i} = 6.0$ case (i.e. slightly above the zero-crossing) are shown in figure 13. The plots show no sign of a mode transition. All k_y contributions are ITG-like, as is especially obvious from the Q_i/Q_e curve, which is smooth and way above TEM levels for all k_y. However, the direction of the particle flux changes sign, implying that the second zero-crossing of Γ—as the first—is due to a spectral balance between inward (this time at low k_y) and outward fluxes (at high k_y), but this time these are both caused by ITG turbulence. As has been shown, this effect is qualitatively captured by the quasilinear model, which relies on only one 'representative' k_y, and although the gradient value of this second zero-crossing in the R/L_{T_i} scan is overestimated by almost 20%, it is obvious that the quasilinear model can be used to (at least qualitatively) describe also this region of parameter space.

The model has so far only been tested for cases with one unstable ITG mode and one unstable temperature gradient

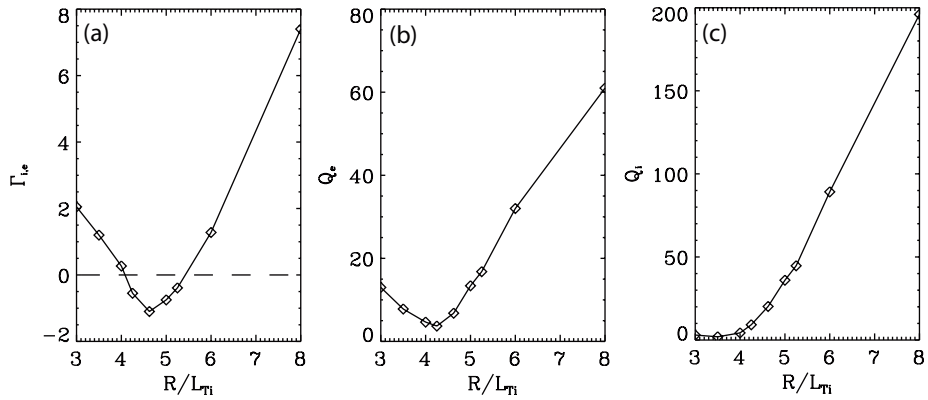

Figure 11. The particle flux (*a*) and the electron and ion heat fluxes (*b*), (*c*) for the reduced density gradient $R/L_n = 2.5$, showing a particle pinch for R/L_{T_i} between 4.1 and 5.5. The dashed line corresponds to $\Gamma = 0$.

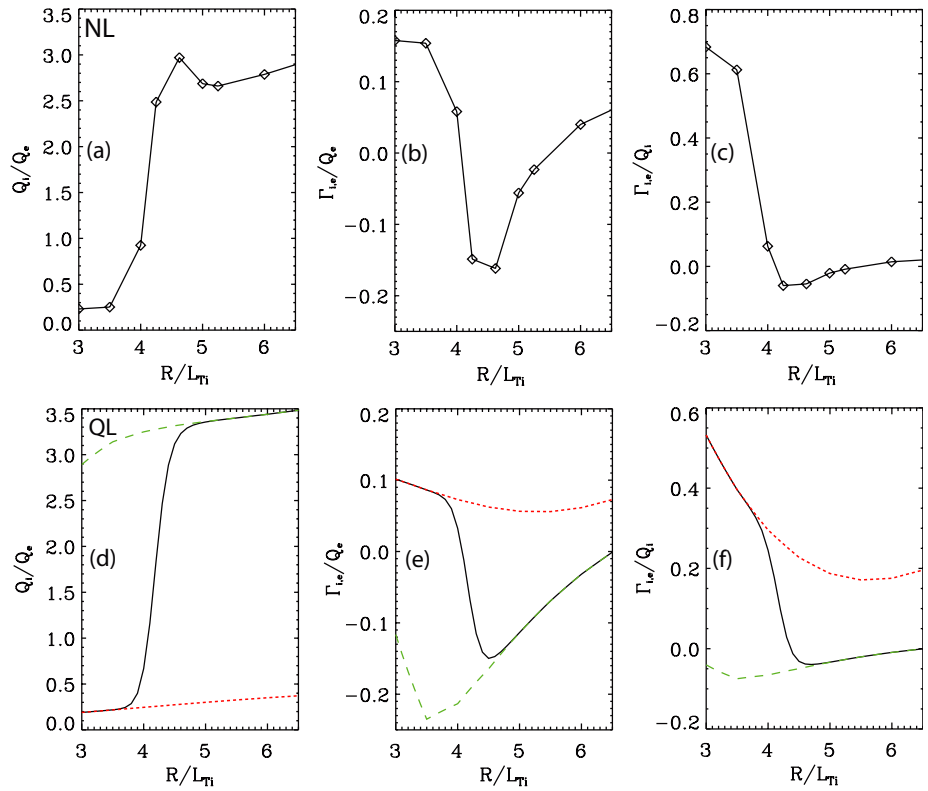

Figure 12. The black curves depict the nonlinear (top) and quasilinear (bottom) ratios of the different fluxes for $R/L_n = 2.5$. The dotted and dashed curves correspond to the values of the underlying TEM and ITG modes, respectively.

driven TEM present, i.e. for moderate normalized temperature and density gradients with $\eta_e > 1$. For these cases, the zonal flows in the TEM regime are weak [7], for fully zonal flow dominated TEM–ITG transitions (i.e. for $\eta_e < 1$) the quasilinear model will probably fail. The model is also expected to fail if the gradients are high enough to drive even more subdominant modes. Preliminary tests that have not been included in this paper show good results also for realistic mass ratio and slightly different temperature ratios.

We finally want to point out that this simple model alone can of course not replace more sophisticated (and more expensive) quasilinear or nonlinear investigations. The strength of the model is that it can be used to identify experimentally accessible regions in higher dimensional parameter space. This information can then be used to select interesting (and experimentally relevant) parameter sets by additional criteria (e.g. by maximizing the gradients, which corresponds to strongly peaked profiles), and use these parameter sets as a starting point for more detailed investigations.

6. Conclusions

We have shown that in situations where TEM and ITG instabilities coexist linearly, features of both microinstabilities may be found in nonlinear simulations. Due to their k_y dependence, different microinstabilities can be dominant at different k_y in the same nonlinear system, leading to a

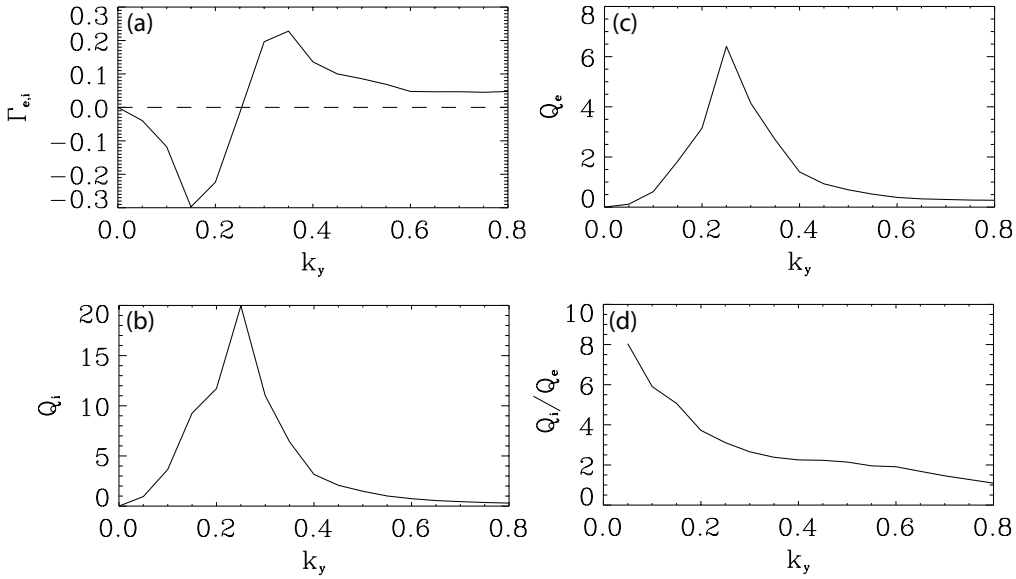

Figure 13. Spectra of the particle flux (*a*), the ion and electron heat fluxes (*b*), (*c*) and the ratio of the ion and electron heat fluxes (*d*) close to the second zero-crossing of the particle flux for $R/L_n = 2.5$ and $R/L_{T_i} = 6.0$. The dashed line in (*a*) corresponds to $\Gamma = 0$.

spectral coexistence of the TEM and ITG turbulence. At the transition point, this coexistence can even be present at a single perpendicular wavenumber, implying that two different frequencies (and even drift directions) are observed for the same spectral mode.

Two mechanisms for the experimentally important condition of zero particle flux have been explored in the TEM–ITG system: the first is a fine-tuned balance of the TEM induced outward transport and the ITG induced particle pinch at different perpendicular wavenumbers. The second is the transition between pinch and outward transport within the ITG dominated regime; this transition is also k_y dependent and thus also allows for a balance between in- and outward transport, similar to the previous case.

It has been shown that the basic phenomena in the nonlinear TEM–ITG system can be described and understood at least qualitatively by a very simple quasilinear model, which only uses the (dominant and subdominant) eigenvalues at a single, 'characteristic' k_y. This simplicity allows for higher dimensional studies of the $\Gamma \approx 0$ (or rather $\Gamma/Q_{e/i} \approx 0$) hypersurface, so that experimentally accessible areas in parameter space with interesting properties can be identified and used as a starting point for more involved (e.g. nonlinear) investigations. This scheme will be employed in future publications.

References

[1] Dimits A. *et al* 2000 Comparisons and physics basis of tokamak transport models and turbulence simulations *Phys. Plasmas* **7** 969–83

[2] Jenko F., Dorland B., Kotschenreuther M. and Rogers B. 2000 Electron temperature gradient driven turbulence *Phys. Plasmas* **7** 1904–10

[3] Ernst D. *et al* 2004 Role of trapped electron mode turbulence in internal transport barrier control in the Alcator C-Mod Tokamak *Phys. Plasmas* **11** 2637–48

[4] Dannert T. and Jenko F. 2005 Gyrokinetic simulation of collisionless trapped-electron mode turbulence *Phys. Plasmas* **12** 072309

[5] Lang J., Parker S. and Chen Y. 2007 Gyrokinetic δf particle simulation of trapped electron mode driven turbulence *Phys. Plasmas* **14** 082315

[6] Merz F. and Jenko F. 2008 Nonlinear saturation of trapped electron modes via perpendicular particle diffusion *Phys. Rev. Lett.* **100** 035005

[7] Ernst D., Lang J., Nevins W., Hoffman M., Chen Y., Dorland W. and Parker S. 2009 Role of zonal flows in trapped electron mode turbulence through nonlinear gyrokinetic particle and continuum simulation *Phys. Plasmas* **16** 055906

[8] Terry P. and Gatto R. 2006 Nonlinear inward particle flux component in trapped electron mode turbulence *Phys. Plasmas* **13** 062309

[9] Ryter F. *et al* 2005 Experimental study of trapped-electron-mode properties in tokamaks: threshold and stabilization by collisions *Phys. Rev. Lett.* **95** 085001

[10] Jenko F. 2004 On the nature of ETG turbulence and cross-scale coupling *J. Plasma Fusion Res. Ser.* **6** 11–16

[11] Candy J., Waltz R., Fahey M. and Holland C. 2007 The effect of ion-scale dynamics on electron-temperature-gradient turbulence *Plasma Phys. Control. Fusion* **49** 1209–20

[12] Görler T. and Jenko F. 2008 Scale separation between electron and ion thermal transport *Phys. Rev. Lett.* **100** 185002

[13] Rewoldt G. and Tang W. 1990 Toroidal microinstability studies of high-temperature tokamaks *Phys. Fluids* B **2** 318–23

[14] Kinsey J.E., Waltz R.E. and Candy J. 2006 The effect of safety factor and magnetic shear on turbulent transport in nonlinear gyrokinetic simulations *Phys. Plasmas* **13** 022305

[15] Estrada-Mila C., Candy J. and Waltz R.E. 2006 Density peaking and turbulent pinch in DIII-D discharges *Phys. Plasmas* **13** 074505

[16] Angioni C., Peeters A., Jenko F. and Dannert T. 2005 Collisionality dependence of density peaking in quasilinear gyrokinetic calculations *Phys. Plasmas* **12** 112310

[17] Fable E., Angioni C. and Sauter O. 2008 Gyrokinetic calculations of steady-state particle transport in electron internal transport barriers *Plasma Phys. Control. Fusion* **50** 115005

[18] Maslov M. *et al* 2009 Density profile peaking in jet H-mode plasmas: experiments versus linear gyrokinetic predictions *Nucl. Fusion* **49** 075037

[19] Roman J E, Kammerev M, Merz F and Jenko F 2010 Fast eigenvalue calculations in a massively parallel plasma

turbulence code *Parallel Comput.* at press http://www.sciencedirect.com/science/article/B6V12-4XY9DD5-1/2/0443d5556

[20] Hammett G. *et al* 1993 Developments in the gyrofluid approach to tokamak turbulence simulations *Plasma Phys. Control. Fusion* **35** 973–85

[21] Cohen B., Williams T., Dimits A. and Byers J. 1993 Gyrokinetic simulation of $E \times B$ velocity-shear effects on ion-temperature-gradient modes *Phys. Fluids* B **5** 2967–80

[22] Dimits A., Williams T., Byers J. and Cohen B. 1996 Scalings of ion-temperature-gradient-driven anomalous transport in tokamaks *Phys. Rev. Lett.* **77** 71–4

[23] Conway G. *et al* 2006 Observations on core turbulence transitions in ASDEX upgrade using doppler reflectometry *Nucl. Fusion* **46** S799–808

[24] Kotschenreuther M. 1995 Quantitative predictions of tokamak energy confinement from first-principles simulations with kinetic effects *Phys. Plasmas* **2** 2381–9

[25] Jenko F., Dannert T. and Angioni C. 2005 Heat and particle transport in a tokamak: advances in nonlinear gyrokinetics *Plasma Phys. Control. Fusion* **47** B195–206

[26] Staebler G., Kinsey J. and Waltz R. 2007 A theory-based transport model with comprehensive physics *Phys. Plasmas* **14** 055909